AIAA AVIATION Forum
12-16 June 2023, San Diego, CA and Online
AIAA AVIATION 2023 Forum

10.2514/6.2023-3479

Investigation of Gas Flow Within a Laser Amplifier Head for Optimal Cooling

Edward Lowell* and Oliver T. Schmidt†
University of California San Diego, La Jolla, California 92093

Frantisek Batysta‡ and Thomas Spinka§
Lawrence Livermore National Laboratory, Livermore, CA, 94550

In an effort to improve thermal management of the gain medium in high-average power, high-intensity lasers, this study focuses on simulating the gas flow through multiple narrow channels. Actively cooling lasers of this class involves flowing helium gas through an array of closely-spaced vanes, where each vane contains a thin slab of gain medium. Since the role of turbulence is crucial to both the thermal management of the gain material and to the optical quality of the laser, it is imperative that the state of the flow within these channels and over the gain medium is properly understood. In the absence of experimental data, the current work utilizes RANS turbulence models and the Langtry-Menter transition prediction model to obtain flow solutions within a representative helium gas-cooled laser amplifier design. The RANS results reveal three flow features within the amplifier head: separation at the inlet diffuser, potential relaminarization within the channels, and a separation region downstream due to the diverging sections of the channels. While computationally inexpensive and suited for exploring optimal aerodynamic design configurations of the amplifier head, the RANS solutions only provide averaged flow quantities. Since the fluctuating density field is necessary for future aero-optical analyses of the laser propagating through the gas flow, a preliminary LES is also introduced. In addition to aero-optics, it is expected the LES will shed light into the inherent unsteadiness of the aforementioned separation regions, which in turn may highlight any links to structural vibrations of the vanes themselves. A comparison of the mean flows of the RANS and LES solutions indicates good agreement within the channels and near the gain medium, and shows that the LES and RANS capture similar separation and recirculation features.

I. Introduction

High-power, high-intensity lasers show promise for new applications in laser-driven high-energy-density science, industry, and medicine. The most pressing technical issue for the next generation of solid-state lasers is thermal management. Typically, multi-slab amplifier design is used to address this cooling problem. Rather than relying on a large, single piece of gain material, this method instead divides the gain medium into multiple thin slabs. Each slab is housed within a vane, where the vanes are stacked and spaced so as to form an array of channels. A representative geometry of these vanes and enclosure is shown in Fig. 1. Gas flowed through these channels extracts heat from the exposed surfaces of the slabs. In comparison to an amplifier consisting of a single slab, this design allows for an increased surface area-to-volume ratio, which in turn promotes improved heat removal while maintaining desired optical properties [1].

Gas cooling is inherently an aperture- and average-power scalable technology, and is utilized in several high energy laser systems to date [2–4]. The early development of this technology for laser slab cooling was led by Albrecht and Sutton, Albrechet et al., and Sutton et al. [5–8] and heat fluxes were of order 1W/cm^2, and cooling efficiency was demonstrated up to ~5W/cm^2. Significant scaling (up to one order of magnitude) of this technology to higher extractable heat fluxes is required to enable the next generation of lasers.

Careful consideration must be made in pursuing this scaling, however. In its passage through the amplifier head, the laser beam propagates through both the gain medium and the cooling gas. Thus, multi-slab amplifiers inherently

*Ph.D. Student, Department of Mechanical and Aerospace Engineering
†Assistant Professor, Department of Mechanical and Aerospace Engineering, AIAA Member
‡Research Staff
§Program Element Leader for Laser Development

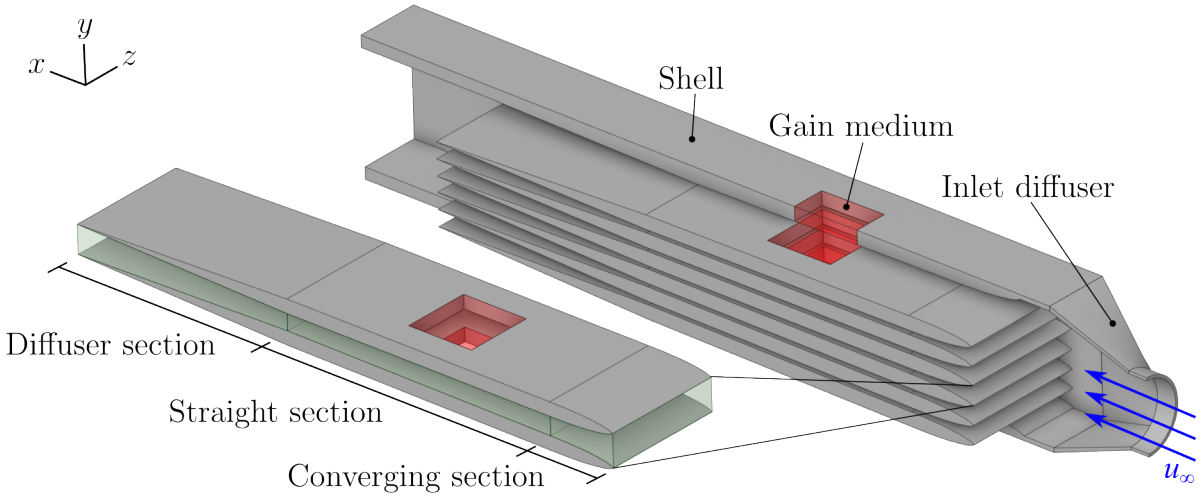

Fig. 1 Representative geometry of a multislab laser amplifier head. The outer shell is cut in order to reveal the array of vanes inside. A channel formed by two vanes is highlighted, and sections of the channel are labeled.

introduce a coupling between the physics of the laser, and that of the gas flow. More specifically, turbulence plays a key role in the link between these two realms. The link stems from the dependence of a gas's index of refraction on its density, which can be described by the relation shown in Eq. (1):

$$n - 1 = (n_{\text{sta}} - 1)\frac{\rho}{\rho_{\text{sta}}}, \tag{1}$$

where n is the refractive index of the gas, ρ is its density, and n_{sta} and ρ_{sta} are the standard refractive index and density at a pressure of 1 bar and a temperature of 0 °C. On one hand, turbulent flow is greatly desired for its ability to efficiently convect heat from the surface of the gain medium. On the other hand, turbulence introduces density fluctuations into the flow, which translate into fluctuations in the index of refraction, and in turn, scattering of the laser beam. Thus, the tremendous requirements for removal of waste heat generated in the optical pumping process, combined with the necessity to maintain the highest optical beam quality, makes amplifier slab cooling of high-average-power solid-state lasers a formidable technological challenge at the intersection of heat transfer, fluid mechanics, and aero-optics.

II. Methodology

In the absence of experimental flow data, Reynolds Averaged Navier-Stokes (RANS) simulations are used to obtain flow solutions within the amplifier head. The motivating factor in using RANS is that it is computationally inexpensive when compared to Large Eddy Simulations (LES), or Direct Numerical Simulations (DNS), and enables simulation of the entire amplifier head. The reduced computational cost also makes RANS an ideal candidate for performing simulations on variations of the base amplifier design in pursuit of an optimized geometry. The availability of transition models for RANS simulations allows for further insight into the state of the flow. This is especially of interest, as early work on this study predicted strong accelerations present within the channels. The presence of these strong accelerations would make the flow susceptible to relaminarization, and could have a significant impact on both the thermal and optical properties of the flow through which the laser beam propagates.

RANS simulations by nature are only able to deliver averaged quantities. Since density fluctuations will be of interest for an aero-optical analysis, the RANS simulations will be backed by a LES. In light of this, a preliminary LES of the entire head is conducted. As simulation of the entire domain using a wall-resolved LES would be infeasible in terms of computational resources, a wall-modeled LES is instead used. Keeping in mind the potential presence of transition and relaminarization, and noting the wall-model's limitations in handling such phenomena, a careful comparison between the RANS and LES mean flows is conducted.

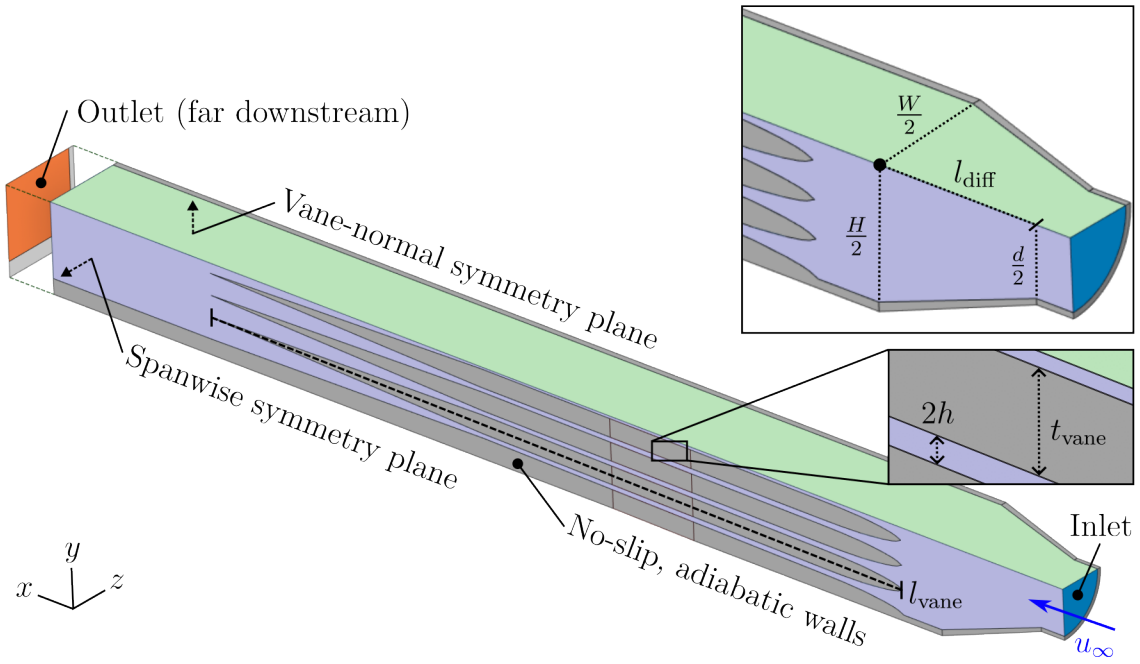

Fig. 2 Quarter of a representative amplifier head. Boundaries are highlighted and dimensions are labeled. Size and parameters of this representative amplifier head (e.g. number of vanes and vane thickness) are not equal to those of the actual simulated domain.

A. Domain and Fluid

The domain for both the RANS and LES is that of the fluid within a representative laser amplifier head. The simulated region consists of a short section of pipe, a circular-to-rectangular inlet diffuser, the channels formed by cooling vanes, and an outlet placed far downstream. The channels formed by the cooling vanes are further categorized into the converging sections, straight-channel sections, and diffuser sections (not to be confused with the diffuser found upstream). Figure 2 illustrates a representative domain. Exact specifications and geometry will vary by application, so representative geometries are used for illustration. The dimensions of the geometry are denoted as h, t_{vane}, L_{vane}, L_{diff}, W, H, and D_{inlet}, for the average channel half-width, vane thickness, vane length, diffuser length, amplifier width (in z), amplifier height (in y), and the inlet diameter, respectively. Relative to each other, the relations between the dimensions are as follows:

$$\frac{t_{\text{vane}}}{h} = O(10)$$
$$\frac{H}{h}, \frac{W}{h}, \frac{L_{\text{diff}}}{h}, \frac{L_{\text{vane}}}{h} = O(10^2)$$
$$H > W > L_{\text{diff}}$$

Helium gas is typically chosen as the coolant of this type of amplifier because it has excellent heat transfer and optical properties; namely, a relatively high thermal conductivity, and an index of refraction near unity. In this case, the domain is Helium gas at a specified background pressure and temperature of 4 bar and 300 K, respectively. Under these conditions, the maximum Mach number achieved in the head is 0.2. In light of this, the flow is assumed to be incompressible for this study. Table 1 summarizes the background conditions and the gas properties.

B. Mesh and Grid Independence

To conduct the grid study, several meshes are created in Ansys Fluent using the poly-hexcore workflow. The $k-\omega$ SST turbulence model is used to obtain the steady state solution on each mesh, and several monitors are used to determine convergence. Figure 3a shows the variation of inlet pressure and maximum streamwise velocity with each of

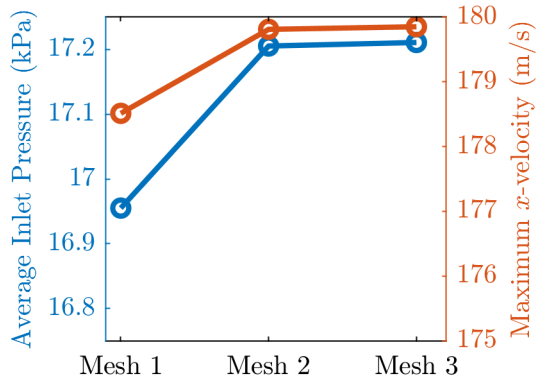

(a) Area-weighted average pressure of the inlet (left, blue) and maximum x-velocity over the domain (right, red) plotted for each level of grid refinement of the RANS mesh.

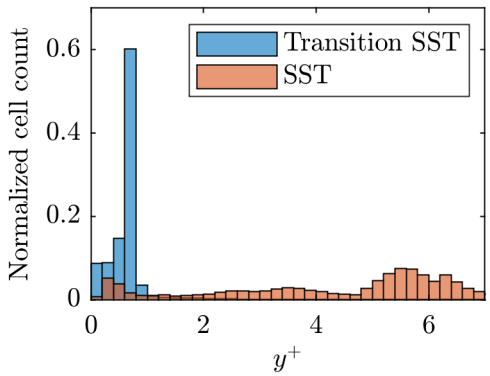

(b) Histogram of y^+ values value over all walls in the domain for both the base SST mesh, and for the Transition SST mesh.

Fig. 3 Grid refinement metrics and boundary layer resolution.

the meshes, and indicates good convergence. A more highly resolved inflation layer is added to the walls of the 12 million cell grid for use in the RANS simulation involving the transition model. The resulting mesh has a cell count of 64 million. Fig. 3b shows that the inflation layer on the mesh used by the transition model satisfies the model's $y^+ \approx 1$ requirement at the walls. Elements with $y^+ > 1$ are found on the trailing edges of the vanes.

C. RANS Simulations

1. Boundary Conditions

Boundary conditions in the RANS simulations consist of a prescribed velocity inlet, pressure outlet, and adiabatic walls. Symmetry is exploited in the vane-normal (y), and span-wise (z) directions to simplify the computational domain. The velocity at the inlet is set to a constant velocity of 65 m/s for the fully turbulent RANS simulation, and switched to a corresponding fully-developed pipe flow profile with 5% turbulent intensity for the simulation with the transition model active. The pressure outlet is set to 0 gauge pressure.

2. Turbulence Models

The $k-\omega$ SST and Transition SST turbulence models are used in this study. The $k-\omega$ SST model is first used to obtain a steady-state solution that is then set as the initial condition for the Transition SST. The Transition SST model, which is based off of the 4-equation model developed by Menter et. al., is used to predict laminar-turbulent transition in fluid flows [9]. It does so by coupling the $k-\omega$ SST model with two more transport equations for intermittency and momentum-thickness Reynolds number, and through the use of empirical correlations. The two additional transport equations are given by:

Table 1 RANS and LES reference values for Helium gas

Property	Reference value
Density, ρ_{ref}	0.642 kg/m^3
Temperature, T_{ref}	300 K
Pressure, p_{ref}	4.0×10^5 Pa
Viscosity, μ_{ref}	2.0×10^{-5} Pa·s
Heat capacity ratio, γ	5/3

$$\frac{\partial(\rho\gamma)}{\partial t} + \frac{\partial(\rho U_j\gamma)}{\partial x_j} = P_{\gamma 1} - E_{\gamma 1} + P_{\gamma 2} - E_{\gamma 2} + \frac{\partial}{\partial x_j}[(\mu + \frac{\mu_t}{\sigma_\gamma})\frac{\partial\gamma}{\partial x_j}] \tag{2}$$

$$\frac{\partial(\rho R\tilde{e}_{\theta t})}{\partial t} + \frac{\partial(\rho U_j R\tilde{e}_{\theta t})}{\partial x_j} = P_{\theta t} + \frac{\partial}{\partial x_j}[\sigma_{\theta t}(\mu + \mu_t)\frac{\partial R\tilde{e}_{\theta t}}{\partial x_j}] \tag{3}$$

The Transition SST model is detailed in the Ansys Fluent theory guide, and in Menter et. al [9, 10]. Default values supplied by Fluent are used for empirical relations.

3. Solver

A second order implicit scheme is used to advance the solution in time, and the SIMPLE scheme accounts for the pressure-velocity coupling. Default under-relaxation factors are used, and second-order upwind schemes are selected for the discretization of all variables. All RANS simulations are performed in Ansys® Fluent, Release 21.1.

D. Large Eddy Simulation

In addition to the RANS component, a preliminary Large Eddy Simulation is conducted in this study. The setup of the LES parallels that of the RANS, in that it assumes the flow is incompressible, and assumes the same domain and analogous boundary conditions. To save on computational costs, an algebraic wall-model is used in order to reduce resolution requirements for the boundary layer mesh. The wall-model is based off of the Shur et al. formulation, which combines a mixing length model with a modified Smagorinsky model, and with the wall-damping function of Piomelli [11–13]. In like fashion to the RANS simulation, the LES advances the solution in time with a second order implicit scheme, and spatially discretizes all variables with a second-order upwind scheme. The SIMPLE algorithm is again used to account for pressure-velocity coupling. All LES simulations are performed in Ansys® Fluent, Release 21.1.

III. Results and Discussion

The flow within the amplifier head exhibits three main flow features in three corresponding regions: the inlet diffuser, channels, and channel diffusers. These features are presented in the following sections, where emphasis is placed on the RANS solution. The preliminary LES results are also presented, where the mean flow solution is compared to that of the RANS simulation.

A. Inlet Diffuser

The inlet to the domain consists of a circular-to-rectangular diffuser. The ratios of the vane-normal and spanwise diffuser lengths to the streamwise length are approximately 2.9 and 2.8, respectively. Figure 4 shows the flow separation on both the spanwise and vane-normal symmetry planes. While the separation region is three-dimensional, it predominately forms on the side wall (aligned with z) and creates a recirculation zone, as indicated by the negative x-velocity component. The separation and subsequent recirculation are attributed to the large diffuser angle, where current dimensions yield an equivalent angle of 72 degrees. This angle tends to be highly inefficient with respect to the resistance coefficient [14].

The separation and recirculation zones not only affect the efficiency of the diffuser, but also the inflow conditions of the channels. Figure 5 shows the streamwise velocity at the inlets to select channels. The recirculation region affects the channels furthest from the lower wall, as is indicated by the large negative streamwise velocities shown in the upper contours. Another interesting feature is that, while the flow in the upper and lower channels tend to be more or less uniform in y, several channels have a spot of high velocity, such as the one shown in the middle of Fig. 5. The downstream effects of these distributions are investigated in the following sections. Overall, while the current geometry of the diffuser is compact and allows for a smaller overall amplifier head, it does so at the expense of diffuser effectiveness. In the case of future design iterations of the amplifier head, flow separation and recirculation at the diffuser can be accounted for in an effort to increase efficiency, and to promote uniformity of the flow through the channels.

B. Channels

The Transition SST model allows for prediction of the onset of transition. This is especially important within the channels where heat transfer and optical transmission are of great concern. The contours of intermittency give an idea

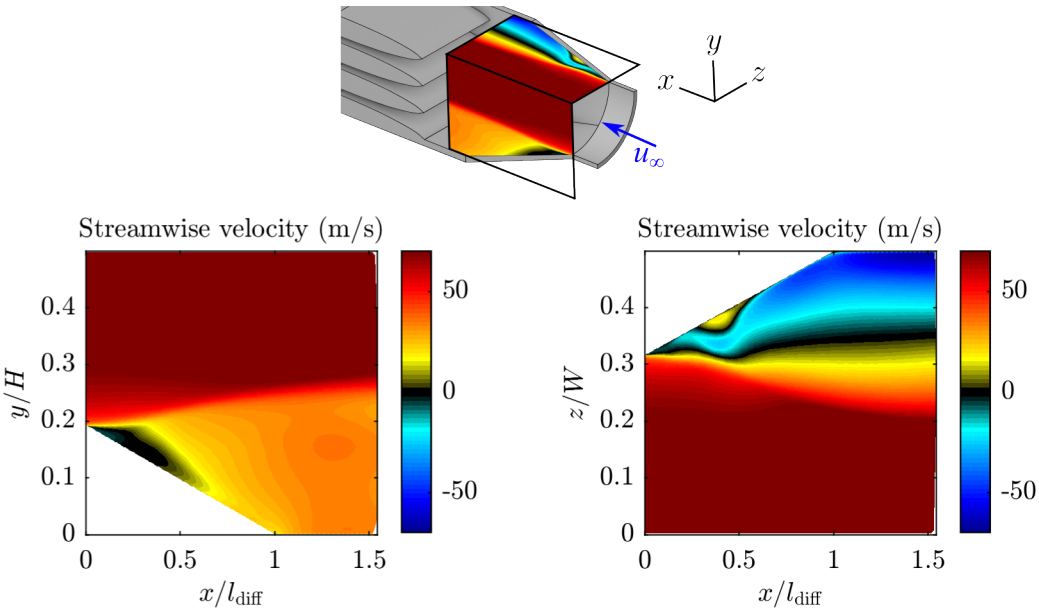

Fig. 4 Streamwise velocity contours on the inlet diffuser. Top figure indicates where the contours lie on the representative domain. Bottom left is the contour on the spanwise symmetry plane, and the bottom right contour lies on the vane-normal symmetry plane.

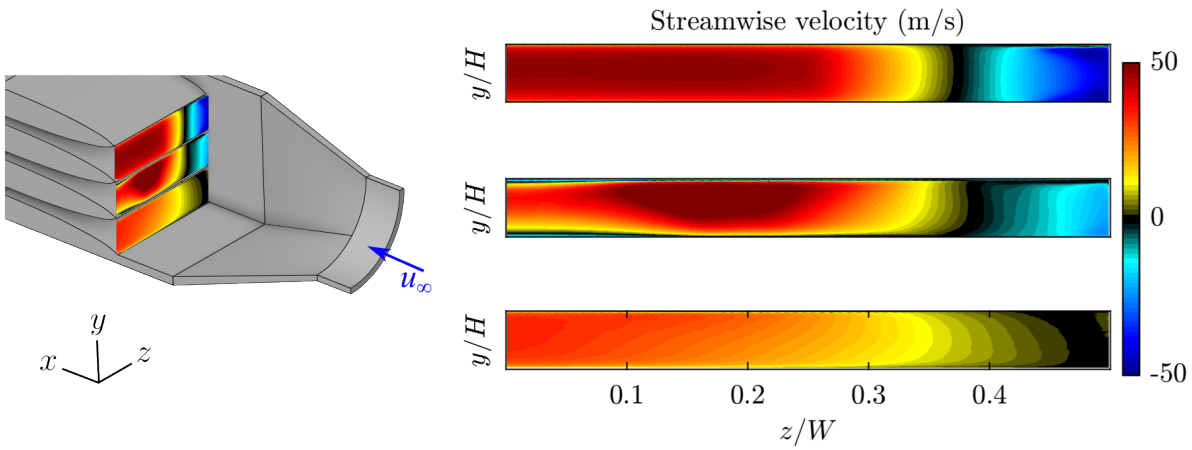

Fig. 5 Streamwise velocity contours plotted at the entrance of several channels. From top to bottom, the channels represent: channel closest to vane-normal symmetry plane, a channel between the vane-normal symmetry plane and amplifier shell, and the channel adjacent to the amplifier wall. Note that the axes are not to scale.

as to the state of the flow, where an intermittency of one corresponds to a fully turbulent flow, and zero corresponds to a laminar flow. The intermittency on the midplanes of several channels are shown in Fig. 6. Focusing on the straight channel section (the region between the two dashed blue lines), it is apparent that much of the flow within the channels is laminar. Only a few channels exhibit transition as shown by the streaks on the contour in the center of Fig. 6. This is an unexpected result, since preliminary estimates indicated that the flow would be turbulent in most of the channels.

Focusing on the regions of the midplanes directly above or below the gain medium, as can be seen within the red outlines in Fig. 6, the state of the flow varies based on which channel is viewed. The channel adjacent to the symmetry plane, (a), shows that the flow relaminarizes further upstream than either of the other channels. The middle channel shows that the flow remains turbulent for much of the area over the amplifier slab. Taking into account all of the vanes (including the ones not shown), the ratio of fully turbulent area to the total area over the amplifier slabs is 45%. In terms of heat transfer, this would indicate that the flow has the potential to improve cooling capability if it transitions to

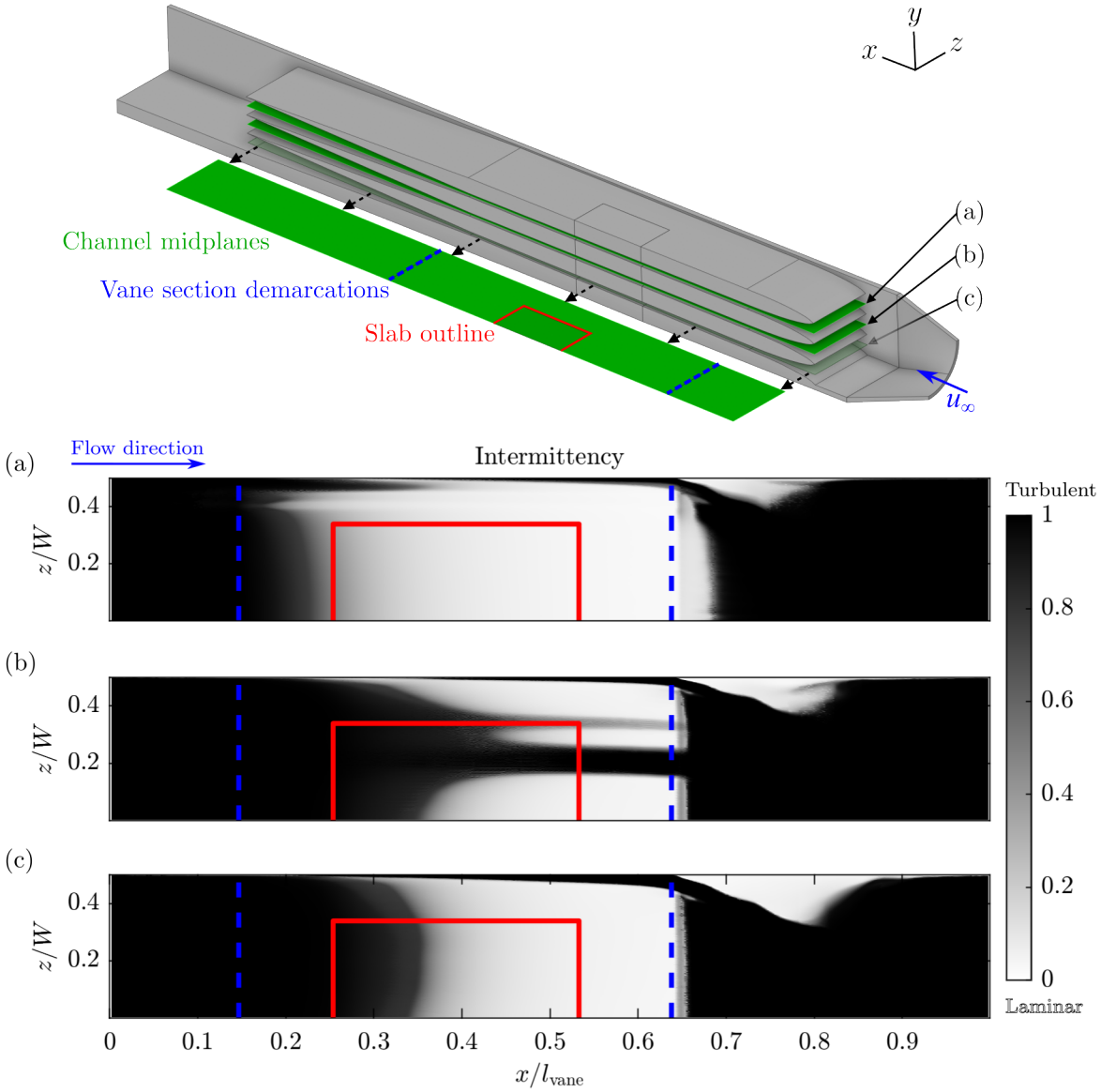

Fig. 6 Intermittency contours plotted at the midplanes of several channels. The blue dotted lines in the contour plots separate the vane into its three parts (in increasing x): converging section, straight section, and diffuser section. The red boxes represent the area above the gain medium. The contours represent: (a) midplane adjacent to vane-normal symmetry plane, (b) a midplane between the vane-normal symmetry plane and amplifier shell, and (c) the midplane adjacent to the amplifier wall. Note that the axes are not to scale.

turbulence in all of the channels.

While not as influential to the optics as the flow near the gain medium, the boundary layer on the sidewalls also shows interesting transition features. The sidewall is located at the top of each contour in Fig. 6, and the boundary layer exhibits both relaminarization and transition - this is especially present in the uppermost plot. The intermittency along the wall begins at 1, transitions to 0, and then back to 1 again. This indicates that the initially turbulent boundary layer at the wall relaminarizes, and then transitions again as it nears the downstream diffuser section (beyond the rightmost dashed blue line).

Since the ability of the flow to remove heat from the amplifier slabs is dependent on the state of the flow within the channels, careful attention to the design details of the amplifier head is important. Further design considerations will need to ensure that relaminarization does not occur, and that a turbulent flow is maintained within the channels.

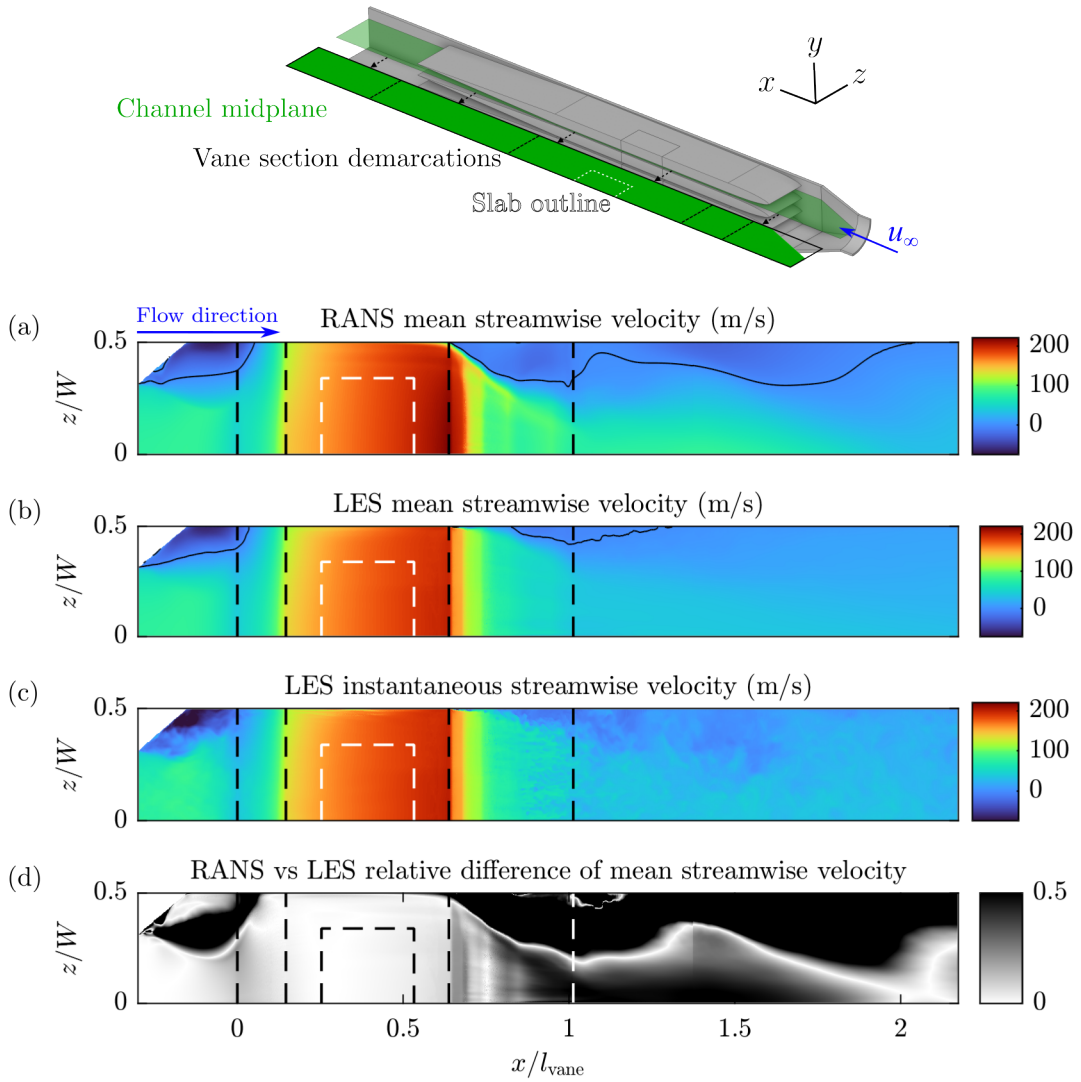

Fig. 7 Comparison between the RANS and LES mean x-velocity profiles on the midplane adjacent to the vane-normal symmetry plane. The solid black lines in (a) and (b) are the contour lines of zero streamwise velocity, while the vertical dashed lines mark the sections of the vane. The dashed square outlines the location of the slab. A snapshot of the LES instantaneous streamwise velocity is shown in (c). The black regions in (d) are portions where the relative difference between the RANS and LES exceed 50%.

C. Downstream Diffusers

The diffuser section of the channels are characterized by separation regions. Notably, the transition model predicts that that flow, which was previously laminar within the channels, transitions to turbulence, as seen in Fig. 6 near the rightmost blue dashed line. While separation occurs off of the vanes themselves, it predominately occurs off of the channel sidewall. The top side of the contours in Fig. 6 show the low intermittency bubbles which form on the sidewall at the beginning of the diffuser section of the channels (right dashed blue line). This indicates the presence of a laminar separation and a turbulent reattachment further downstream. Figure 7 shows the x-component of velocity over an extended region of the vane-normal symmetry plane, with a contour line indicating where the x-velocity is zero. Once the flow exits the diffuser, the contour tends towards the wall, but separates and reattaches further downstream. This occurs on other midplanes, though not as pronounced.

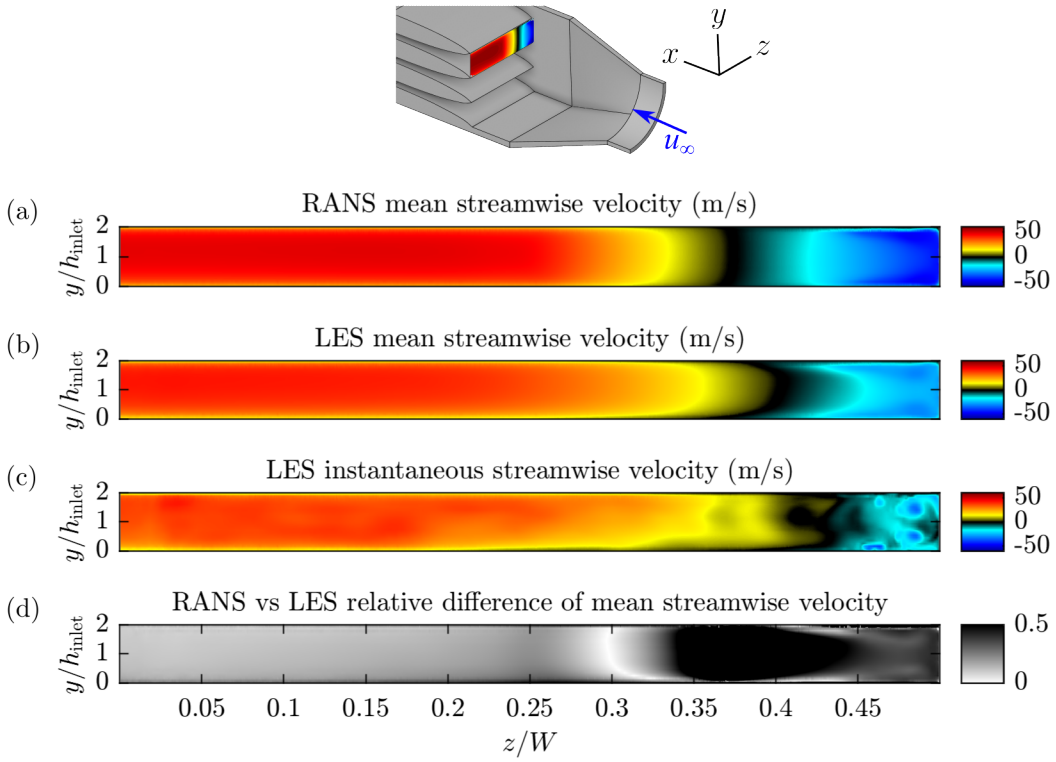

Fig. 8 Comparison between the RANS (a) and LES (b) mean x-velocity profiles on the channel inflow plane adjacent to the vane-normal symmetry plane. The solid black lines in (a) and (b) are the contour lines of zero streamwise velocity, while the vertical dashed lines mark the sections of the vane. The dashed square outlines the location of the slab. A snapshot of the LES instantaneous streamwise velocity is shown in (c). The black regions in (d) are portions where the relative difference between the RANS and LES exceed 50%.

D. Comparison between RANS and LES

An LES is conducted on the same domain using the same mesh as that used in the RANS study. While the mesh may be coarse in terms of an LES, it is used for an initial comparison between the two models. The LES and RANS mean flows are compared while keeping in mind the limitations of the LES wall-model in capturing the potential presence of transition and relaminarization.

The LES predicts a similar mean flow as the RANS, as presented in Fig. 7 and 8. The black contour lines in (a) and (b) represent the lines of zero streamwise velocity. These outline the regions where separation and recirculation occur. As shown, both the RANS and LES predict the separation region at the entrance of the diffuser, as well as the separation that begins in the channel diffuser section. By inspection, the upstream curves are comparable. However, the downstream separation regions are slightly different between the two simulations. The RANS predicts a steeper separation, as well a reattachment point further downstream when compared to the LES.

In looking at the relative difference of the flows, as shown in Fig. 7 (c), it can be seen that the majority of the regions in the contours are below 50%. In fact, the majority of the mean flow within the straight section of the channels is consistent between the two simulations, with relative differences below 10%. This is a good sign, in that the LES and RANS for the most part show agreement for the flow over the gain medium, which is the main region of interest. This is even in the presence of discrepancies between the two simulations as indicated by the large regions of high relative difference upstream and downstream of the straight channel sections. An upstream discrepancy can be seen in Fig. 8, where the channel inflow streamwise velocity is plotted. As seen in the relative difference, the disparity is slightly larger, where the majority of the region has a relative difference of approximately 10% or greater, and a larger discrepancy as to the shape of the recirculation region. These differences are not unexpected, however, as they occur in the highly transient areas of the domain.

Overall, the RANS and LES show excellent agreement in the mean flow at the region of interest - namely the straight channel sections, and the area near the gain medium. This is in light of the upstream and downstream mean

flows showing larger differences, and with the inherent limitations of the LES wall-model in picking up transition and relaminarization effects.

IV. Conclusion

Current results from the RANS transition model show three major flow structures within the amplifier head. The upstream diffuser causes a large separation and recirculation zone which in turn reduces its efficiency, and causes the distribution of the flow into the channels to be non-uniform. More importantly, the transition model predicts that the flow within the channels and over the gain medium is not fully turbulent as initially predicted. Rather, the majority of the flow remains laminar, with only several channels exhibiting transition to turbulence in certain regions. The diffusers downstream also present a large separation region off of the sidewall. These separation regions are of interest as they not only impact the flow, but their unsteady nature could lead to vibrations of the vane structures themselves. Comparison of the RANS results and LES results show good agreement between the mean flows within the straight sections of the channels. This is true even with the presence of the upstream and downstream discrepancies, and with the LES wall-model's inherent limitations in capturing transition and relaminarization effects. Further simulations of the domain are in progress, where the flow is instead considered compressible, and boundary conditions on the slabs are implemented so as to simulate heating of the gain material by the laser. This will yield flow solutions with the required density fluctuations for an aero-optical analysis.

Acknowledgments

OTS and EL gratefully acknowledge support by the U.S. Department of Energy under FES Award DE-SC0021339 (PM Kramer Akli). This work was performed under the auspices of the U.S. Department of Energy by Lawrence Livermore National Laboratory under Contract DE-AC52-07NA27344, was supported by the LLNL-LDRD Program under Project No. 20-ERD-006 and from HEP and ARDAP under award SCW1648. LLNL-CONF-848976.

References

[1] Mason, P. D., Fitton, M., Lintern, A., Banerjee, S., Ertel, K., Davenne, T., Hill, J., Blake, S. P., Phillips, P. J., Butcher, T. J., Smith, J. M., Vido, M. D., Greenhalgh, R. J. S., Hernandez-Gomez, C., and Collier, J. L., "Scalable design for a high energy cryogenic gas cooled diode pumped laser amplifier," *Appl. Opt.*, Vol. 54, No. 13, 2015, pp. 4227–4238.

[2] Haefner, C., Bayramian, A., Betts, S., Bopp, R., Buck, S., Cupal, J., Drouin, M., Erlandson, A., Horáček, J., Horner, J., et al., "High average power, diode pumped petawatt laser systems: a new generation of lasers enabling precision science and commercial applications," *Research Using Extreme Light: Entering New Frontiers with Petawatt-Class Lasers III*, Vol. 10241, International Society for Optics and Photonics, 2017, p. 1024102.

[3] Mason, P., Divokỳ, M., Ertel, K., Pilař, J., Butcher, T., Hanuš, M., Banerjee, S., Phillips, J., Smith, J., De Vido, M., et al., "Kilowatt average power 100 J-level diode pumped solid state laser," *Optica*, Vol. 4, No. 4, 2017, pp. 438–439.

[4] Albach, D., Loeser, M., Siebold, M., and Schramm, U., "Performance demonstration of the PEnELOPE main amplifier HEPA I using broadband nanosecond pulses," *High Power Laser Science and Engineering*, Vol. 7, 2019, p. e1.

[5] Albrecht, G., and Sutton, S., "Gas cooling of laser disks," *Energy Technol. Rev.*, 1988.

[6] Albrecht, G. F., Sutton, S. B., Robey, H. F., and Freitas, B. L., "Flow, heat transfer, and wavefront distortion in a gas cooled disk amplifier," *High Power and Solid State Lasers II*, Vol. 1040, International Society for Optics and Photonics, 1989, pp. 37–55.

[7] Albrecht, G. F., Robey, H. F., and Erlandson, A. C., "Optical properties of turbulent channel flow," *Applied optics*, Vol. 29, No. 21, 1990, pp. 3079–3087.

[8] Sutton, S., Albrecht, G., and Robey, H., "Heat removal in a gas cooled solid-state laser disk amplifier," *AIAA journal*, Vol. 30, No. 2, 1992, pp. 431–435.

[9] Menter, F. R., Langtry, R. B., Likki, S., Suzen, Y., Huang, P., and Völker, S., "A correlation-based transition model using local variables—part I: model formulation," 2006.

[10] Fluent, A., "ANSYS fluent theory guide 15.0," *ANSYS, Canonsburg, PA*, Vol. 33, 2013.

[11] Shur, M. L., Spalart, P. R., Strelets, M. K., and Travin, A. K., "A hybrid RANS-LES approach with delayed-DES and wall-modelled LES capabilities," *International journal of heat and fluid flow*, Vol. 29, No. 6, 2008, pp. 1638–1649.

[12] Smagorinsky, J., "General circulation experiments with the primitive equations: I. The basic experiment," *Monthly weather review*, Vol. 91, No. 3, 1963, pp. 99–164.

[13] Piomelli, U., Moin, P., and Ferziger, J. H., "Model consistency in large eddy simulation of turbulent channel flows," *The Physics of fluids*, Vol. 31, No. 7, 1988, pp. 1884–1891.

[14] Idelchik, I., *Flow resistance: a design guide for engineers*, Routledge, 2017.